Received: 23 December 2020 | Revised: 13 April 2021 | Accepted: 18 April 2021

High Voltage

DOI: 10.1049/hve2.12108

ORIGINAL RESEARCH PAPER

# Effect of sinusoidal waveform and frequency on space charge characteristics of polyimide

Hanwen Ren[1] | Yasuhiro Tanaka[2] | Hiroaki Miyake[2] | Qingmin Li[1] | Haoyu Gao[1] | Chengqian Li[1] | Zhongdong Wang[3]

[1]State Key Laboratory of Alternate Electrical Power System with Renewable Energy Sources, North China Electric Power University, Beijing, China

[2]Tokyo City University, 1-28-1 Tamazutsumi, Setagaya, Tokyo, Japan

[3]School of Electrical and Electronic Engineering, The University of Manchester, Manchester, UK

**Correspondence**

Qingmin Li, State Key Laboratory of Alternate Electrical Power System with Renewable Energy Sources, North China Electric Power University, Beijing, 102206, China.
Email: lqmeee@ncepu.edu.cn

Associate Editor: Jin Li

**Funding information**

Natural Science Foundation of Beijing Municipality, Grant/Award Number: 3202031; National Natural Science Foundation of China, Grant/Award Numbers: 51737005, 51929701

## Abstract

The charge phenomena under sine and half-wave sine voltages within the frequency range of 500 Hz are studied here. Based on the pulsed electro-acoustic method, the traditional circuit design under high-frequency voltages is first analysed. It is found that the selection of a 186 pF protection capacitor and a 333 kΩ protection resistor can ensure that the actual voltage applied to the sample is consistent with the expected input. Based on this design, experimental results show that the polarity of the charge accumulated in the depth of the sample is determined by that of the upper electrode. Comparison results under special voltages with different amplitudes and frequencies indicate that the amount of accumulated charge under sine voltages are larger than those under positive and negative half-wave sine and DC conditions, and the samples under lower-frequency conditions show more charge accumulation. The maximum electric field strengths appear at 90 and 270 degrees of the sine voltage with a frequency of 10 Hz, and their values are 68.55 and 81.82 kV/mm, respectively. Therefore, the charge characteristics are easily affected by the voltage's waveform and frequency parameters. The results obtained here can provide guidance for the application of insulating materials under special voltage environments.

## 1 | INTRODUCTION

During the daily operation of high-voltage equipment, it usually faces several insulation problems including electric tree generation, partial discharge, and dielectric breakdown which can directly cause insulation ageing and degradation [1–3]. A key factor leading to these phenomena is the severe distortion of the electric field. The accumulation of space charge inside solid insulation is the main factor causing electric field distortion, which has also become an important indicator for evaluating the dielectric properties and operating states of different materials [4–6]. The evaluation of charge accumulation mainly relies on accurate measurement techniques.

At present, the technologically advanced measurement methods are mainly of two types: the first type is used for measuring the total charge amount and the type for measuring space charge distribution. The former is based on the current integration charge method which can obtain the changing process of the total charge amount flowing through the sample. This method is only used for DC voltages at present [7, 8]. The measurement methods for charge distribution mainly include the pulsed electro-acoustic (PEA) method, thermal methods and pressure wave methods [9, 10]. Among them, the PEA method has a relatively mature measurement principle and recovery algorithm. It has been widely used in charge measurements under DC and AC voltages within a power frequency. Due to the different injection barriers of electrons and holes at electrode interfaces and trap depths inside samples, the charge distribution inside insulating materials depends on the voltage's waveform and polarity [11–13]. Therefore, carrying out research on the charge characteristics under the voltage

conditions faced by equipment insulation will help analyse the charge problems withstood by the equipment.

Different from traditional power equipment operating in DC and AC voltages at a power frequency, the fast-developing power electronic equipments such as motors and power electronic transformers usually face special voltage conditions including high-frequency sine and pulse voltages. Researchers have found that the insulation subjected to these special stresses may deteriorate rapidly within 1–2 years [14–16]. Therefore, some charge measurements aiming at special voltage conditions have also been accomplished. The charge characteristics of cross-linked polyethylene materials under unipolar half-wave sine and rectangular wave conditions are discussed in [17]. It is indicated that the accumulated charge amount under some special voltages is more than that under DC conditions, and the voltage frequency can affect charge distribution. The charge characteristics of polyamide-imide (PAI) materials under positive and negative DC, rectangular wave and half-wave sine voltages are studied in [18, 19]. It is also found that compared with the results under DC conditions, electric field distortion is more serious under some special voltage environments. The charge results of PAI, polyester-imide and polyimide (PI) films commonly used as coating materials are further compared under different rectangular wave conditions [20]. It is indicated that PI materials show little charge accumulation. However, there is no further comparative research on the charge properties of PI material under half-wave sine, sine and other voltage conditions. PI material is one of the important insulating supports for power electronic equipment including motors and power electronic transformers. A more comprehensive charge research on this material will help in further improvement and application.

According to the above analysis, we mainly compare the charge phenomena of PI films under half-wave sine, sine and DC voltages. Based on the analysis of the electrode design suitable for high-frequency conditions, we compared the results of charge accumulation and distorted electric field of Kapton-type PI materials under the effect of voltage amplitude and frequency parameters. Then, we summarised the accumulation law of space charge under these special voltage conditions.

## 2 | THE MEASUREMENT SYSTEM BASED ON THE PEA METHOD

The measurement principle of the PEA method is shown in Figure 1. Under the effect of the applied high voltage, space charge can be injected and accumulated inside the sample. Meanwhile, the applied pulse voltages can disturb the charge layer in the balanced state. The charge then vibrates and thus, an acoustic wave is generated. Finally, the acoustic wave propagates to the piezoelectric transducer and is converted into an electrical signal, which is measured by the oscilloscope [21]. In the figure, $R_{dc}$ and $C_c$ are the protection resistor and capacitor, respectively. $\rho_s(x)$ and $\rho(x)$ represent the charge density. $\sigma(d_s)$ and $\sigma(0)$ are the two induced surface charges. $d_s$ is the sample thickness. $E(x)$ is the electric field distribution inside the sample. $v_{out}(t)$ is the measured signal.

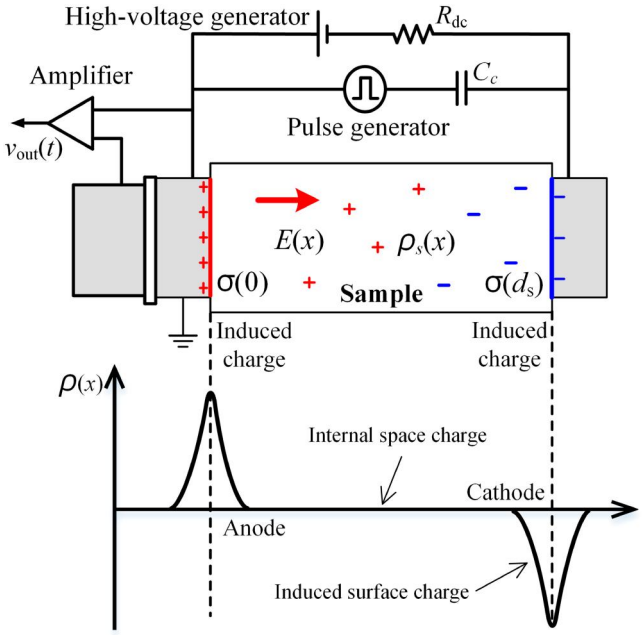


**FIGURE 1** The basic principle of pulsed electro-acoustic method

From Figure 1, the measured waveform using the PEA method mainly contains three parts: the space charge accumulated inside the sample, the surface charges induced at the two interfaces between the electrodes and the sample. In the actual measurement, due to the effect of pulse excitation and transducer, the measurement resolution is usually at the level of a few microns. Therefore, the waveform of surface charge always broadens in the measurement, and its shape is close to the Gaussian waveform shown in Figure 1. When the space charge inside the sample accumulates in the vicinity of the electrode interface, it can overlap with the surface charge waveform due to the resolution.

The actually established PEA system is shown in Figure 2(a). The materials of the two electrodes contacted with the sample are the semi-conductive layer and aluminium, respectively. The former is used to match the acoustic impedance of the sample. The polyvinylidene fluoride (PVDF) material is used as the piezoelectric transducer. To control the measurement process, a self-designed computer programme is accomplished. The computer signals can trigger the output of the pulse generator and the high-voltage generator. Then, the trigger signal from the pulse generator can ensure the synchronization of the oscilloscope record. Finally, the measured voltage signal is calibrated by a recovery algorithm to obtain the actual charge distribution in the measured sample.

The system is used to measure the charge phenomena under two special voltages shown in Figure 2(b). Due to the large random noise in the actual measurement, 100-1000 groups of continuously measured waveforms need to be averaged to obtain the results with a high signal-to-noise ratio. We use 200 groups in the following measurement. For DC voltages, a smooth waveform is obtained every 5 s. For the half-wave sine and sine conditions in Figure 2(b), two measurements

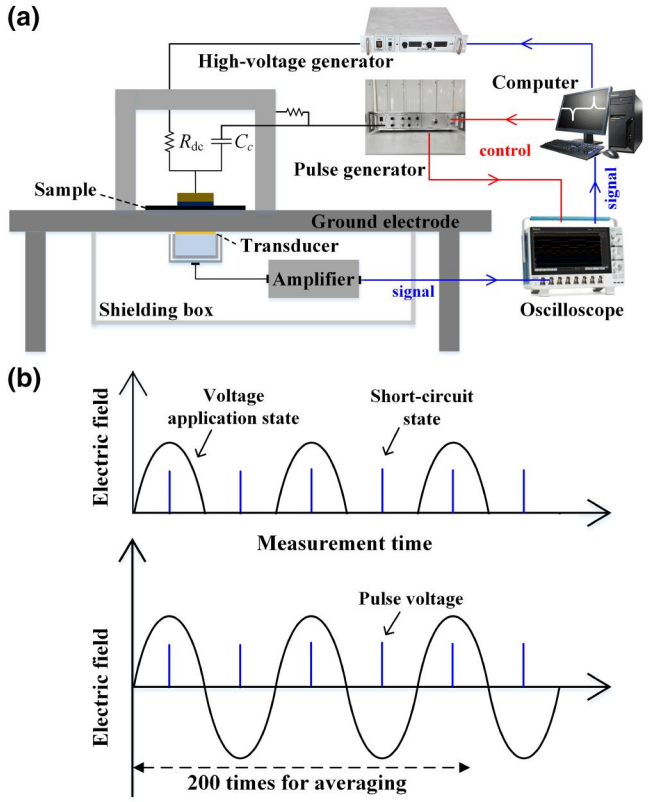


**FIGURE 2** The actual measurement process based on the pulsed electro-acoustic system. (a) The established PEA system and (b) the measurement method for special voltages

are performed in one period of the voltage. The voltage application and short-circuit stages in the half-wave sine voltage are defined as volt-on and volt-off states, respectively. The pulse excitation in the volt-on state is applied at the maximum amplitude of the voltage. In the case of sine voltage, only the charge results at 90 and 270° are obtained. 200 measured results for each state are averaged to obtain smooth waveforms.

According to the IEC standard [22], the half-value width of the induced surface charge peak at the grounded electrode side is defined as the spatial resolution, as shown in Figure 1. The spatial resolution in length can be calculated by multiplying the time resolution and the acoustic velocity in the sample. For our established PEA system, the spatial resolution is about 12 μm. Due to the resolution, the capacitance charges at the interfaces formed by the electrodes and the sample always broaden to the Gaussian shape, as shown in Figure 1. The corresponding width of the rising and falling edges of the surface charge waveform is about 12 μm in our system. The accumulated internal space charge in the vicinity of the electrode interfaces is always superimposed with the surface charge signal in the PEA measurement results. In the following measurements, we use the Kapton-type PI materials with the thickness of 125 μm from DuPont company as the measured samples. Due to the broadened surface charge waveforms at the interfaces, the internal space charge distribution within the range of 100 μm can be properly shown without the superimposition effect of capacitance charges. In addition, the following experiments under various voltage conditions are all carried out at room temperature.

## 3 | IMPROVEMENT OF THE PEA SYSTEM FOR HIGH-FREQUENCY VOLTAGES

In order to ensure effective measurements using the PEA method, the IEC standard gives the following design method of the electrode circuit, as shown in Figure 3 [22]. $R_p$ in the figure is the resistance of the pulse generator. $V_p$ represents the voltage output from the pulse generator. $C_{sa}$ is the sample capacitance. *Vs* is the output from the high-voltage generator. *Vm* is the voltage actually applied to the sample.

To ensure that a high DC voltage can be accurately applied to the sample following traditional application methods, the standard suggests that the capacitance of the protection capacitor should be less than 1 nF. Its value is usually selected according to the sample capacitance. The resistance of the protection resistor should be larger than 10 kΩ. However, to reduce the impact of accidental breakdown or flashover on the equipment safety, a 1 MΩ resistor is usually chosen to protect the system. Based on these parameter settings, the charge measurements under traditional DC and AC voltages at a power frequency can be accurately realized.

Take the high-frequency sine voltages as an example to analyse the applicability of this parameter selection. A simulation based on the circuit in Figure 3 is constructed, and the output of the high-voltage generator and the actually applied voltage to the sample are compared. The thickness of the PI films selected in the experiments is 125 μm. The diameter of the upper electrode is 5 mm. Therefore, the corresponding capacitance of the sample can be calculated by Equation (1),

$$C_{sa} = \frac{\varepsilon_0 \varepsilon_r S}{d} \tag{1}$$

where $\varepsilon_r$ is the relative permittivity of the sample. $\varepsilon_0$ is the vacuum dielectric constant. $S$ is the effective area. $d$ is the thickness of the sample.

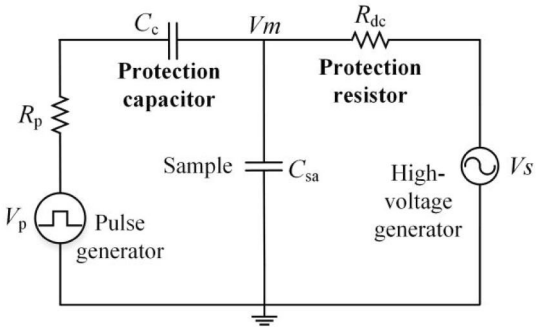


**FIGURE 3** The equivalent circuit of the pulsed electro-acoustic system

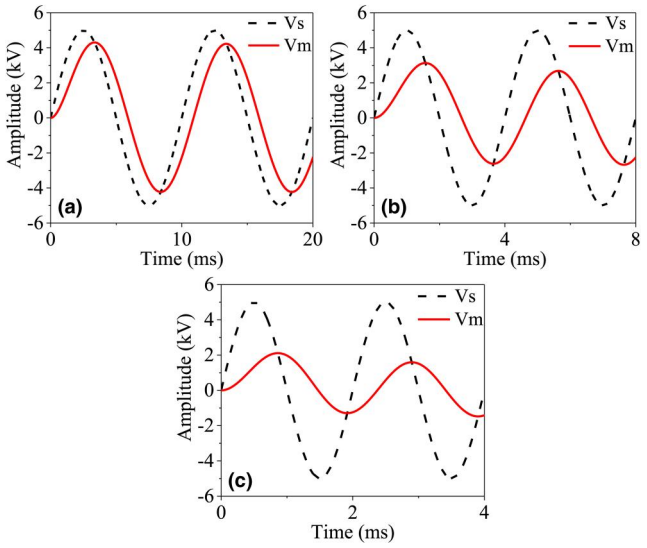


**FIGURE 4** The actually applied voltages to the sample under the traditional circuit design. (a) 100 Hz, (b) 250 Hz, (c) 500 Hz

The calculated capacitance of the PI sample is 4.87 pF. Combined with the simulation circuit in Figure 3, the parameters of the protection capacitor and the resistor are set as 1 nF and 1 MΩ, respectively. Then, the simulated results under an applied sine voltage are obtained, as shown in Figure 4. The amplitude of the applied high voltage is 5 kV.

From Figure 4, when the system traditionally used for DC conditions is directly utilised in high-frequency sine voltages, the actually applied voltages to the sample are significantly different from the outputs from the generator. The difference also increases with frequency. Therefore, the system must be improved for this situation.

The parameter selection of the protection capacitor and resistor actually determines the voltage applied to the sample. In order to analyse the effect of these two components quantitatively, the resistance $R_{all}$ of the whole circuit in Figure 3 is represented by Equation (2),

$$R_{all} = R_{dc} + \frac{1}{j\omega C_{sa}} \Big/ \Big/ \left(\frac{1}{j\omega C_c} + R_p\right) = R_{dc} + \frac{j\omega R_p C_c + 1}{j\omega C_c + (j\omega R_p C_c + 1) j\omega C_{sa}} \quad (2)$$

where $\omega$ is the angular frequency.

The voltage applied to the sample can be then calculated, as shown in Equation (3).

$$V_m = V_s - R_{dc} \cdot V_s / R_{all} \quad (3)$$

An example calculation is given here to show the effect of these two components. The frequency and amplitude of the sine voltage are set as 500 Hz and 500 V, respectively. Then, the voltage applied to the sample is calculated under varying parameters of the protection capacitor and resistor, as shown in Figures 5 and 6. For the sake of simplicity, only the calculated amplitude at 90° is shown by Figure 5. Figure 6 shows the phase difference between the voltage applied to the sample and the high voltage from the generator.

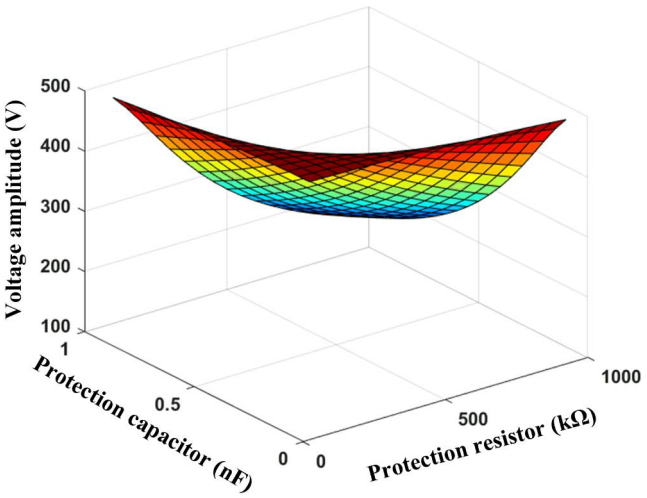


**FIGURE 5** The amplitude of the voltage applied to the sample

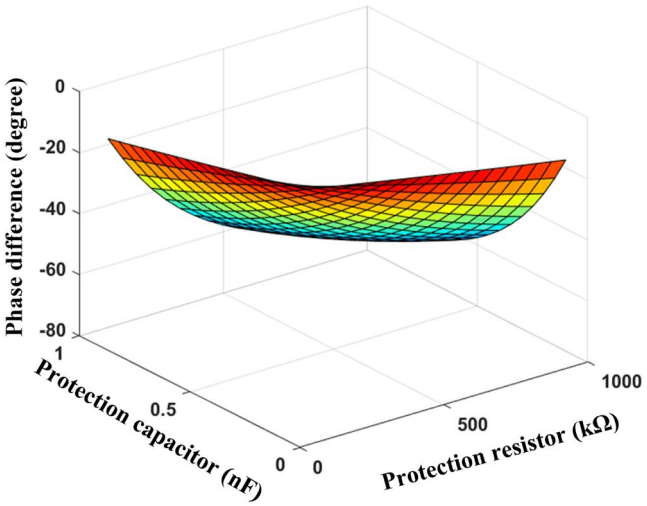


**FIGURE 6** The phase difference between the voltage to the sample and the high voltage from the source

From the figures, when the values of the protection resistor and capacitor decrease, the amplitude of the voltage applied to the sample becomes closer to 500 V and the phase difference becomes closer to 0. However, a smaller value of the protection component means a larger current inside the circuit, which limits the applicable voltage amplitude to protect the measurement system. Combining the available capacitors and resistors in the laboratory, we set three 1 MΩ resistors in parallel and three 560 pF capacitors in series to improve the system. Then, the parameters of the protection resistance and capacitance are 333 kΩ and 187 pF, respectively. The three capacitors are connected in series to reduce the probability of surface flashover along its surface. Based on these selections, the calculated results are shown in Figure 7.

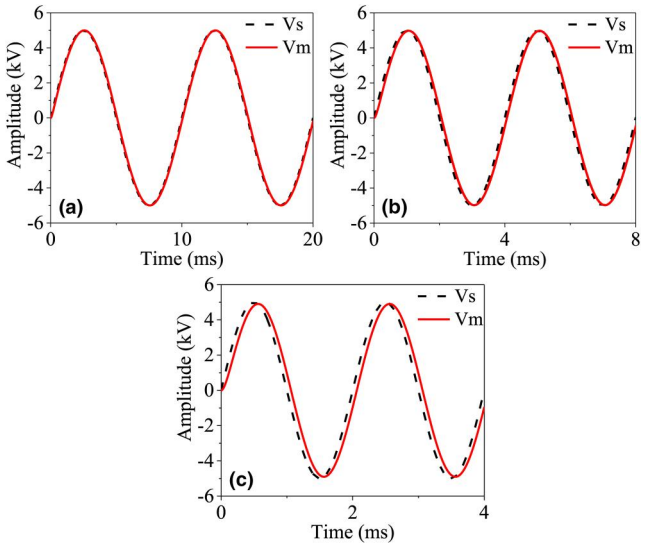


**FIGURE 7** The actually applied voltages to the sample under the improved circuit design. (a) 100 Hz, (b) 250 Hz, (c) 500 Hz

From Figure 7, the actually applied voltages to the sample under this parameter setting are basically close to the output from the generator. Meanwhile, it has been verified that the pulse generator can also be well protected in this system. The voltage from the high-voltage generator is mainly applied to the protection capacitor in Figure 3, which is very close to the waveform Vm in Figure 7. Only a few microvolts are applied to the pulse generator. Therefore, this new system can be used in charge measurements under sine voltages within the frequency of 500 Hz.

## 4 | MEASURED RESULTS AND DISCUSSION UNDER DIFFERENT VOLTAGE CONDITIONS

### 4.1 | Charge phenomena under different voltage amplitudes

For the charge accumulation phenomena under sine and half-wave sine voltages, the effect of voltage amplitude is first analysed. Figure 8 shows the charge results under half-wave sine voltages with two polarities. The field strength labelled in the figure corresponds to the maximum amplitude of the applied voltages, and the frequency is 50 Hz.

From Figure 8, at each amplitude level of the positive voltages a small amount of positive charge is accumulated inside the sample, which is injected from the upper electrode. Under the negative situation, the injection of positive and negative charges occurs on both sides of the electrode, and the migration distance of the negative charge is larger. Since the two electrodes contacted with the sample are aluminium and a semi-conductive layer respectively, the injection and extraction barriers of the two kinds of charges at the two electrode interfaces are different. Meanwhile, from the results based on quantum chemical calculation in [23], the trap sites in the PI

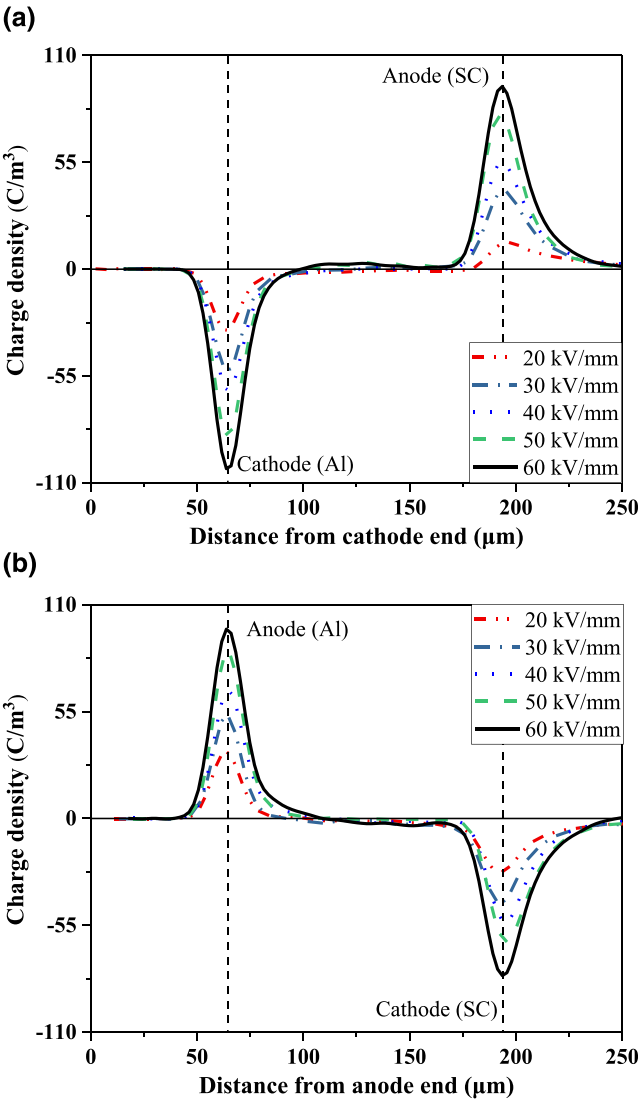


**FIGURE 8** The charge results under two half-wave sine voltages. (a) positive half-wave sine, (b) negative half-wave sine

materials that capture positive and negative charges are 4.4'diaminodiphenyl ether and pyromellitic dianhydride structures, respectively. Due to the different depths of the trap sites, the migration speeds of the two charges are not the same. Thus, their migration distances are also different.

Further, the experimental results at 90 and 270 degrees of the sine voltages are obtained, as shown in Figure 9.

In Figure 9, the polarity of the charge accumulated in the samples under the sine voltages is the same as that of the applied voltage at the time of measurement. It means the charge is mainly injected from the semi-conductive layer, and the accumulation of hetero-charge is formed near the grounded electrode due to the existence of the interfacial barrier. The maximum distortion of the electric field also appears at this position. The amount of accumulated negative charge is larger at 270°. Meanwhile, compared with the results under unipolar half-wave sine voltages in Figure 8, the accumulated charge amount under the sine conditions is larger. Therefore, the

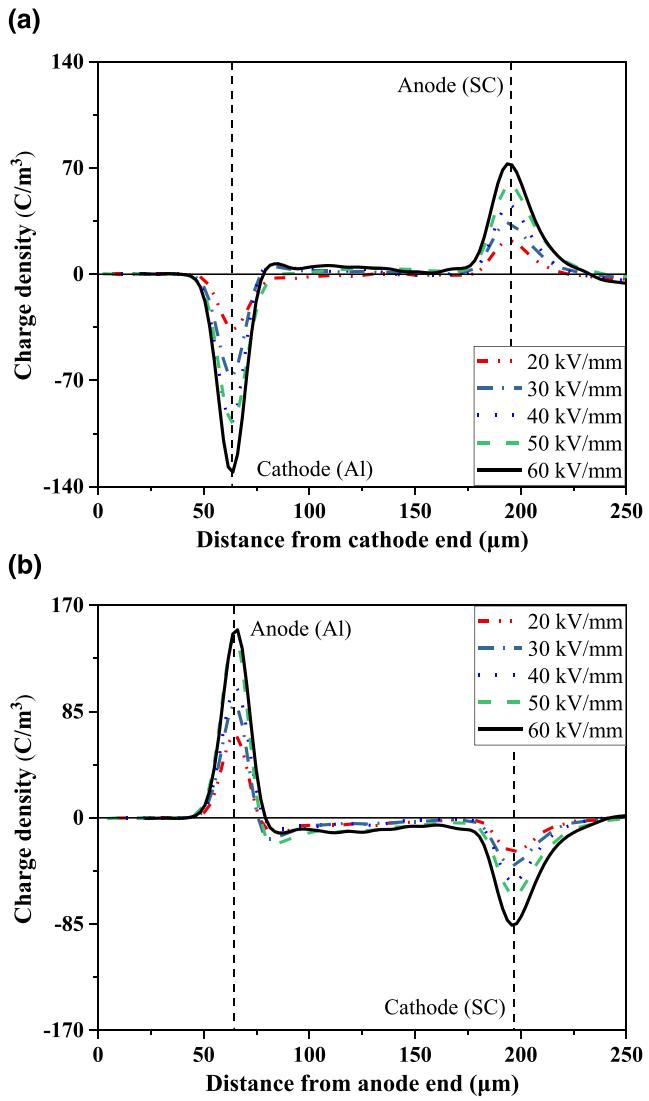


**FIGURE 9** The charge results under sine voltages. (a) 90°, (b) 270°

polarity reversal in the sine voltage makes the PI material withstand a more serious charge accumulation problem. In addition, both the results of the studied PI material under half-wave sine and sine voltages show a large charge accumulation. Before observing the charge phenomena under these PI materials, we also analyse the characteristics of the PET material. It is found that the PET material shows little charge accumulation under half-wave sine and sine voltages with low frequencies and high amplitudes. Therefore, we think that the insulating property of the material itself determines its charge performance under these special voltage conditions.

The distorted electric field distributions under the three kinds of voltages are compared, as shown in Figure 10. The amplitude of the applied electric field is 60 kV/mm, and the field distributions at 90 and 270 degrees of the sine voltage are shown.

From Figure 10, affected by the accumulation of space charge inside the sample, the internal electric field is distorted severely under different voltage conditions. Among them, the

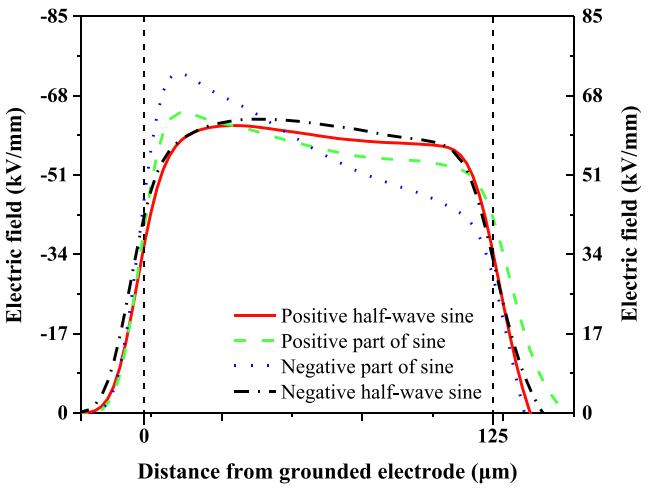


**FIGURE 10** The distorted electric fields under different applied voltages

charge amount under the positive and negative half-wave sine voltages in Figure 8 is little, and the corresponding maximum electric fields are only 61.57 and 62.96 kV/mm. In contrast, larger maximum field strengths are found under the sine voltages, which are 64.49 and 72.76 kV/mm at 90 and 270°, respectively. Both the values appear near the electrode interfaces. Therefore, the polarity reversal in the sine voltages makes the PI material more prone to deterioration and ageing in the negative half part.

## 4.2 | Comparison of charge results under DC and half-wave sine voltages with different frequencies

The charge phenomena under positive and negative DC voltages are first analysed, as shown in Figure 11. Both the field strengths are 60 kV/mm. The ordinate on the left side of the figure corresponds to the thickness direction of the sample. The labels Al and SC represent an aluminium electrode and a semi-conductive layer, respectively. The area of the sample inside is between these two electrodes. The abscissa indicates the measurement time, and the colour represents the accumulated charge amount.

In Figure 11, homo-charges are injected from the two electrode sides under the positive DC voltage. However, after a thirty-minute measurement, there is still no net charge accumulation in the depth of the sample. In contrast, under the negative voltage, positive charge injected from the anode dominates inside the sample, which does not change significantly during the entire measurement time. It means the charge accumulation quickly stabilises under negative DC voltages.

The charge phenomena under half-wave sine voltages with different polarities are then compared, as shown in Figure 12. The amplitude of the applied field strength is 60 kV/mm, and the frequency ranges from 10 to 500 Hz. For the results at one frequency, the left figure corresponds to the volt-on state of

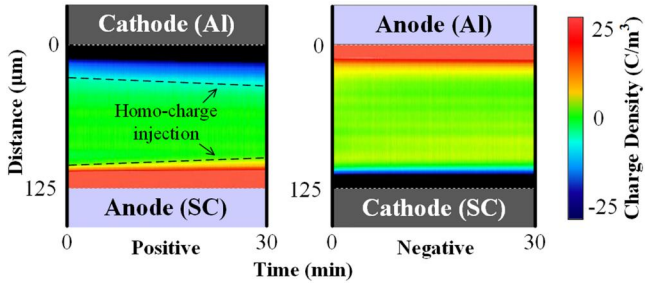


**FIGURE 11** The charge results under DC voltages

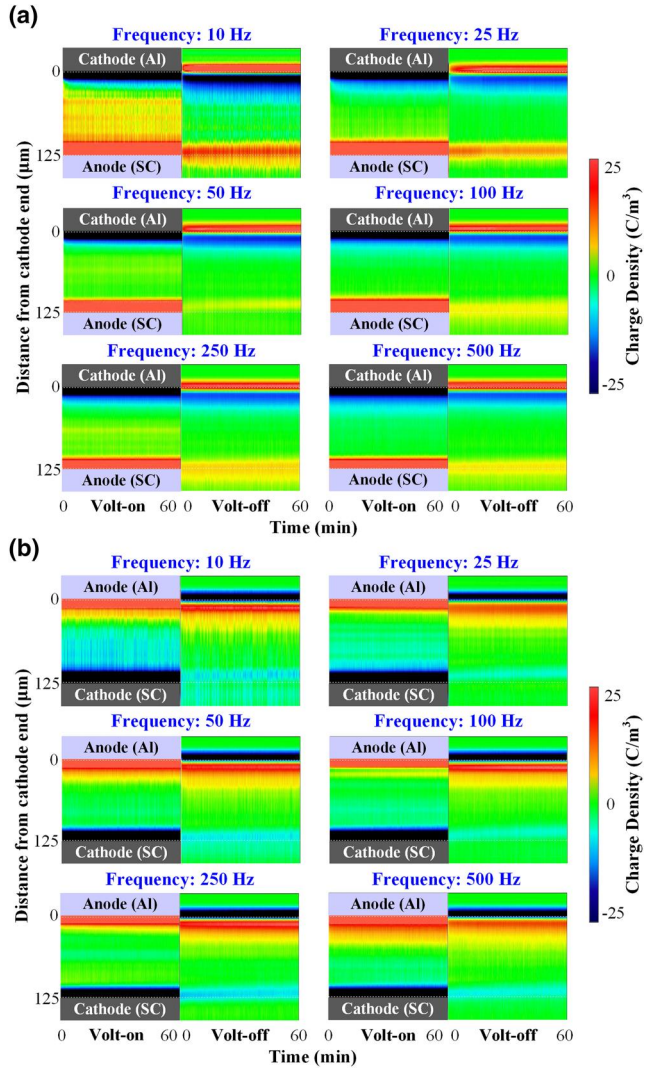


**FIGURE 12** Charge results under half-wave sine voltages with different frequencies. (a) positive half-wave sine, (b) negative half-wave sine

voltage application, and the right one is the volt-off state of short circuit. All the results at the volt-on state are obtained at 90 degrees of the voltages applied.

The results under positive and negative half-wave sine voltages show similar phenomena. At the volt-on stage of 10 Hz, a large amount of charge accumulates under the two half-wave sine voltages, and the charge polarity is consistent with that of the semi-conductive layer. However, after the stage is switched to the volt-off part, the net charge inside the depth of the sample tends to zero. Only some homo-charges can be found near the two boundaries, and it shows more charge accumulation near the aluminium electrode. Therefore, we can infer that the charge injection and extraction barriers on the semi-conductive layer side are lower than those on the aluminium electrode, and the rapid injection and migration of charges occur when a high voltage is applied or when it becomes zero. When the frequency of the applied voltage further increases, the results only show the injection and accumulation of space charge in the vicinity of the electrodes. It is difficult for the charge to migrate to the deep of the sample.

Based on the above charge results, the electric field distributions inside the sample under different DC and half-wave sine voltages can be calculated, as shown in Figure 13.

Consistent with the charge results in Figure 12, according to Figure 13, the maximum field strengths under the two half-wave sine voltages appear at the frequency of 10 Hz. The values are 68.02 and 66.82 kV/mm under the positive and negative conditions, respectively. The field strengths under the other frequency conditions are relatively close. In contrast, the maximum field strengths under positive and negative DC voltages are 63.76 and 65.59 kV/mm, respectively. It means the electric field distortions are close under the negative DC and half-wave sine voltages with the frequency of 10 Hz. However, the PI material under positive half-wave sine voltages is subjected to more severe electric field distortion.

## 4.3 | Space charge and electric field distributions under sine voltages

The charge results under sine voltages with different frequencies are measured, as shown in Figure 14. For the results at one frequency, the left figure corresponds to 90°, and the right one is the result at 270°. The amplitude of the field strength applied to the sample is 60 kV/mm.

From the results in Figure 14, although the accumulated charge inside the sample is injected from the upper electrode, the charge phenomena are different at the two degrees. At 90°, a large amount of charge accumulates in the frequency range of 10-250 Hz, but the amount is little at 300 Hz. At 270°, it can be found that the amount of accumulated charge basically decreases with frequency, and the amount becomes very little when the frequency reaches 300 Hz. Combined with the charge phenomena in Figure 12, the polarity of the applied voltage at the measurement moment determines that of the accumulated charge. This phenomenon indicates that the speed of charge injection, migration and extraction in this PI material is very fast. Meanwhile, homo-charge still remains near the aluminium electrode during the short-circuit stage in Figure 12. Therefore, the results in the two figures indicate that the charge injection and migration speed from the semi-conductive layer side is faster, and the injection and extraction barriers on this

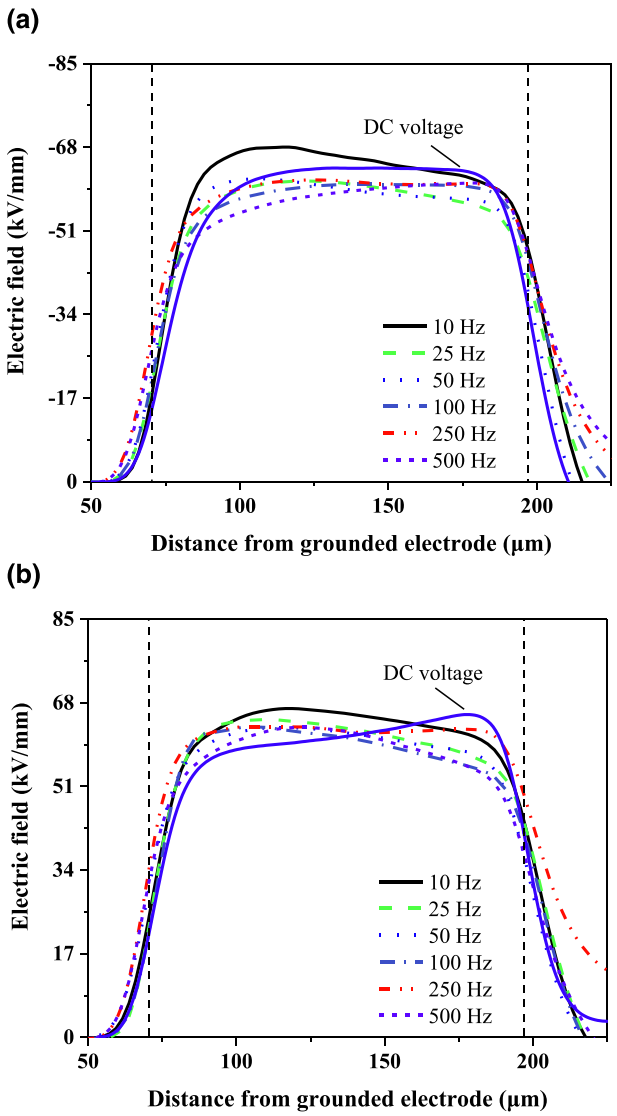


**FIGURE 13** The electric field distributions under DC and half-wave sine voltages. (a) positive half-wave sine, (b) negative half-wave sine

side are lower when a high voltage is applied. For the interfaces formed by the electrodes and the insulating material, the injection and extraction barriers determine the injection and extraction behaviour of the electrons and the holes. The barrier is determined by the vacuum level of the electrodes and the Fermi level of the insulating material. This characteristic can be evaluated by quantum chemical calculations. Based on the calculated results of some materials in [24], the electron and hole barriers at the semi-conductive layer side could be equal to or smaller than those at the aluminium electrode side. Meanwhile, these values can further change due to the interfacial electrical field affected by the applied voltage and accumulated charge. The barriers of the studied PI material will be discussed under different voltage conditions by quantum chemical calculations in the future.

From the charge distribution, the distorted electric field distributions under the above sine conditions are obtained, as shown in Figure 15.

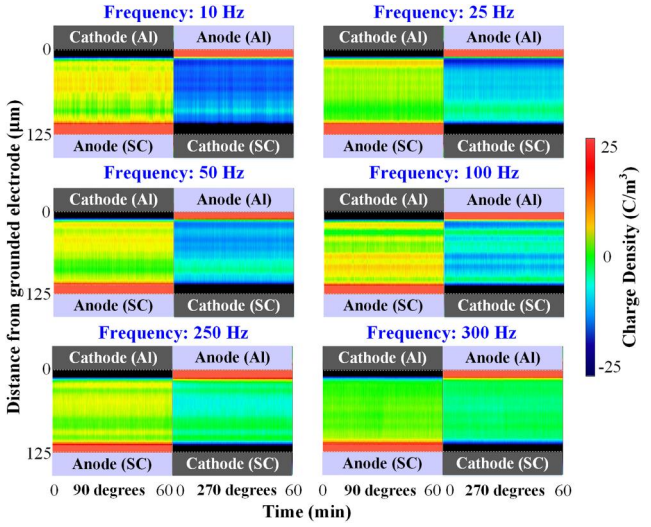


**FIGURE 14** The charge results at 90° and 270° under different sine voltages

The maximum field strength at 90° appears under the voltage condition of 10 Hz, which is 68.55 kV/mm. At 300 Hz, due to little charge accumulation, there is almost no distortion of the internal electric field. The maximum electric fields at other frequencies are relatively close. The distortion of electric field at 270° is basically inversely proportional to the voltage frequency. The maximum strength at the frequency of 10 Hz is about 81.82 kV/mm.

Combined with the results in the above sections, although the frequency parameter can affect the characteristics of charge accumulation and electric field distortion under different voltage conditions, the problem of charge under special voltage conditions can still seriously affect the dielectric properties of PI materials, just like DC voltages. The problem of accumulation under sine voltages is the most serious, and the maximum distortion of electric field appears in the negative half period. The phenomenon and mechanism of charge accumulation under special voltage conditions still need more in-depth research.

## 5 | DISCUSSION

In the above measurement results, the speed of charge accumulation inside the depth of the sample under half-wave sine and sine voltages is very quick after voltage application. Meanwhile, after the high voltage is removed, the charge in the depth also dissipates quickly. Similar charge phenomena are also found in our previous research studies under DC and polarity reversal conditions [25–28], which found that the charge accumulation also appears at the beginning of the voltage application or state transition.

This kind of charge accumulation is mainly due to the rapid migration speed of space charge. According to the measurement research by Dissado [29, 30], an accumulated charge with a high migration speed also exists in the sample.

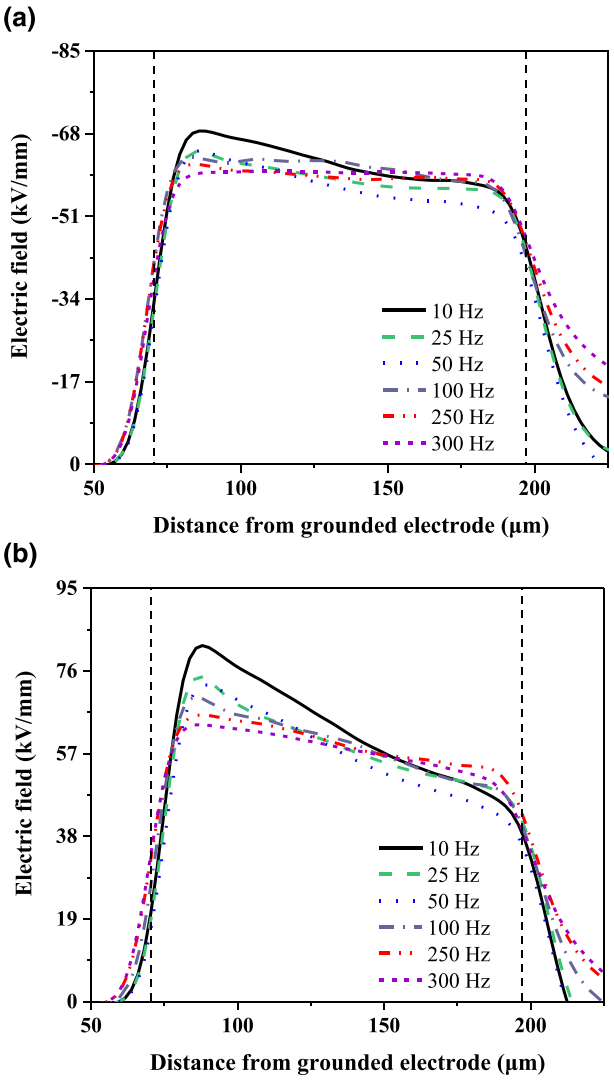


**FIGURE 15** The distorted electric fields under the sine voltages with different frequencies. (a) 90°, (b) 270°

The mobility of this kind of charge is close to $10^{-9}$ $m^2/(Vs)$. Due to the fast charge accumulation, similar phenomena can also be found at the beginning of the voltage application in the references. Meanwhile, the effect of DC-superimposed pulsed electric field is studied in [31]. It is found that when the pulsed voltage transfers between the falling and rising edges, the accumulated charge amount inside the sample decreases or increases sharply. Besides these direct charge measurements, the research based on electric current measurement in [32] also indicates that some parts of space charge can migrate very quickly.

This rapid accumulation phenomenon may be due to the forces withstood by the space charge. Besides the applied electric field force applied to the sample, the space charge also withstands the material force from the attraction of other charges, the material itself and other forces. As shown in Figure 16, when the space charge is in a constant voltage environment, it may accumulate for a long time. In this state, although the researchers have also found rapid charge

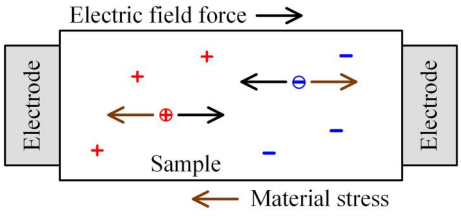


**FIGURE 16** The forces withstood by the space charge

migration in different materials [29, 30], the mobility of most space charge is still in the range of $10^{-17}$ to $10^{-13}$ $m^2/(Vs)$. When the sample is suddenly connected to a high voltage or in a varying electric field, the space charge cannot always keep a balanced state due to the slow changing speed of material stress. Therefore, the space charge may show a larger mobility under special voltage conditions.

## 6 | CONCLUSION

(1) Aiming at the charge measurement under high-frequency voltage conditions, the applicability of traditional electrode design of the PEA system previously used for DC conditions is first simulated and studied. It is found that using the original circuit selections of 1 nF protection capacitor and 1 MΩ protection resistor, the waveform and amplitude of special voltages actually applied to the sample can be deformed significantly. After adjusting the two components to 187 pF and 333 kΩ, the voltage actually applied to the sample is consistent with the expected input within the frequency range of 500 Hz.

(2) The measured results under 50 Hz half-wave sine and sine voltages with different amplitudes show that the homocharge injected from the upper electrode can accumulate in the depth of the sample. The amount of accumulated charge at 90 and 270 degrees of sine voltages is much more than that under half-wave sine conditions. Affected by the accumulated space charge, the maximum electric field strengths under positive and negative half-wave sine voltages are 61.57 and 62.96 kV/mm, respectively. In contrast, the values reach 64.49 and 72.76 kV/mm in the two half periods of sine voltages.

(3) Based on the charge phenomena within the frequency range of 10-500 Hz, it is found that space charge can migrate and distribute in the depth of the sample under the two half-wave sine voltages with the frequency of 10 Hz, while the amount of accumulated charge is relatively smaller at a higher voltage frequency. The PI material under low-frequency sine conditions also shows a large amount of space charge, but it reduces after the frequency reaches 300 Hz. Meanwhile, the maximum electric field strengths under these special conditions are much larger than those under DC voltages. Therefore, the charge accumulation mechanism and dielectric performance evaluation under special voltage conditions for power electronic equipment still need further research.

## ACKNOWLEDGMENTS

We would like to thank the support from the National Natural Science Foundation of China (Grant No. 51929701, 51737005) and Beijing Natural Science Foundation (3202031).

## ORCID

*Hanwen Ren* https://orcid.org/0000-0002-8956-4413

## REFERENCES

1. Hu, S., et al.: Surface-modification effect of MgO nanoparticles on the electrical properties of polypropylene nanocomposite. High Voltage. 5(3), 249–255 (2020)
2. Du, B., et al.: Improved DC conductivity and space charge characteristics of XLPE for HVDC cable application: effect of voltage stabilizers. IEEE Access. 7, 66576–66583 (2019)
3. Khaled, U., Beroual, A., Khan, Y.: Statistical investigation of AC breakdown voltage of natural ester with electronic scavenger additives. IEEE Trans. Dielect. Electr. Insul. 26(6), 2012–2018 (2019)
4. Myneni, S.B., et al.: Investigation on space charge and charge trap characteristics of gamma-irradiated epoxy micro-nano composites. High Volt. 5(2), 191–201 (2020)
5. Hussain, R., Moxter, J., Hinrichsen, V.: Influence of temperature and electric field strength on the space charge behaviour of liquid silicone rubber with carbon black nanofillers. IEEE Trans. Dielect. Electr. Insul. 27(2), 427–432 (2020)
6. Liang, H., et al.: Improved space charge transport model in bi-layer dielectrics-considering carrier dynamic equilibrium. High Voltage. 5(2), 176–183 (2020)
7. Takada, T., et al.: New diagnostic method of electrical insulation properties based on current integration. IEEE Trans. Dielect. Electr. Insul. 24(4), 2549–2558 (2017)
8. Wang, W., et al.: Current integrated technique for insulation diagnosis of water-tree degraded cable. IEEE Trans. Dielect. Electr. Insul. 25(1), 94–101 (2018)
9. Wang, Y.N., et al.: Research progress on space charge measurement and space charge characteristics of nanodielectrics. IET Nanodielectrics. 1(3), 114–121 (2018)
10. Imburgia, A., et al.: Review of space charge measurement systems: acoustic, thermal and optical methods. IEEE Trans. Dielect. Electr. Insul. 23(5), 3126–3142 (2016)
11. Li, J., et al.: Deep trap sites suppressing space charge injection in polycyclic aromatic compounds doped XLPE composite. IET Nanodielectrics. 1(3), 10–13 (2020)
12. Ren, H., et al.: Numerical simulation of the space charge accumulation inside solid insulation subjected to special polarization conditions. Phys. Scr. 95(4) 045807 (2020)
13. Tian, J., Zhou, Y., Wang, Y.: Simulation of space charge dynamics in low-density polyethylene under external electric field and injection barrier heights using discontinuous galerkin method. IEEE Trans. Dielect. Electr. Insul. 18(5), 1374–1382 (2011)
14. Nguyen, M.Q., et al.: Investigations on dielectric properties of enamelled wires with nanofilled varnish for rotating machines fed by inverters, In: IEEE Electrical Insulation Conference and Electrical Manufacturing & Coil Winding Conference, Montreal. pp. 377–381. (2009)
15. Oliver, J.A., Stone, G.C.: Implications for the application of adjustable speed drive electronics to motor stator winding insulation. IEEE Electr Insul Mag. 11(4), 32–36 (1995)
16. Bonnett, A.H.: Analysis of the impact of pulse-width modulated inverter voltage waveforms on AC induction motors. IEEE Trans. on Ind. Applicat. 32(2), 386–392 (1996)
17. Wang, X., et al.: Study of space charge accumulation property in polyethylene under applied voltage of square wave, In: International Conference Electrical Materials and Power Equipment, Guangzhou. pp. 178–181. (2019)
18. Mima, M., Miyake, H., Tanaka, Y.: Measurement of space charge distribution in polyamide-imide film under square wave voltage practical environment for inverter-fed motor, In: IEEE International Conference Dielectrics, Budapest. pp. 1–4. (2018)
19. Takizawa, K., et al.: Space charge behaviour in covering insulating material for motor windings under applied voltage of square wave, In: International Symposium on Electrical Insulating Materials, Niigata. pp. 409–412. (2014)
20. Mima, M., Miyake, H., Tanaka, Y.: Dependence of duty ratio of square wave voltage on space charge accumulation property in motor winding coating insulating material, In: International Conference on the Properties and Applications of Dielectric Materials, Xi'an. pp. 102–106. (2018)
21. Ren, H., Li, Q., Wang, Z.: An improved calibration method for the measurement of space charge inside insulating materials. IEEE Trans. Instrum. Meas. 69(4), 1652–1663 (2020)
22. IEC/TS 62758: Calibration of space charge measuring equipment based on the pulsed electro-acoustic (PEA) measurement principle. International Electrotechnical Commission, Geneva (2012)
23. Takada, T., et al.: Determination of charge-trapping sites in saturated and aromatic polymers by quantum chemical calculation. IEEE Trans. Dielect. Electr. Insul. 22(2), 1240–1249 (2015)
24. Takada, T., et al.: Space charge accumulation in double-layer dielectric systems-measurement methods and quantum chemical calculations. IEEE Electr Insul Mag. 35(5), 36–46 (2019)
25. Negishi, M., et al.: Space charge accumulation in coating materials for motor windings under DC high voltage, In: IEEE International Conference on Condition Monitoring and Diagnosis, Bali. pp. 122–125. (2012)
26. Kasuga, H., et al.: Charge accumulation characteristics of XLPE under DC stresses with semi-conductive electrodes, In: International Conference on Electrical Materials and Power Equipment, Xi'an. pp. 14–19. (2017)
27. Sato, K., et al.: Measurement of space charge distribution in epoxy resin package at high temperature under high DC stress, In: IEEE International Workshop on Integrated Power Packaging, Toulouse. pp. 30–35. (2019)
28. Tanaka, Y., et al.: Space charge accumulation characteristics in super engineering plastics under DC stress at high temperature, In: IEEE Conference on Electrical Insulation and Dielectric Phenomena, Washington. pp. 793–796. (2019)
29. Montanari, G.C., Fabiani, D., Dissado, L.A.: Fast charge pulses: the evidence and its interpretation, In: IEEE International Conference on Solid Dielectrics, Bologna. pp. 10–14. (2013)
30. Xu, M., et al.: Supporting the electromechanical nature of ultra-fast charge pulses in insulating polymer conduction, In: International Symposium on Electrical Insulating Materials, pp. 1–11. Kyoto (2011)
31. Zhang, T., et al.: Space charge behaviour in cable insulation under a DC-superimposed pulsed electric field, In: IEEE International Conference on High Voltage Engineering and Application, Beijing. pp. 1–4. (2020)
32. Zheng, F., et al.: Study of ultra-fast space charge in thin dielectric films, In: Annual Report Conference on Electrical Insulation and Dielectric Phenomena, Shenzhen. pp. 287–290. (2013)

**How to cite this article:** Ren, H., et al.: Effect of sinusoidal waveform and frequency on space charge characteristics of polyimide. High Volt. 6(5), 760–769 (2021). https://doi.org/10.1049/hve2.12108